International Journal of Microwave and Wireless Technologies

cambridge.org/mrf

Novel DC-biasing circuits with arbitrary harmonics-control capability for compact high-efficiency power amplifiers

Shinichi Tanaka, Tomoya Oda and Kento Saiki

Graduate School of Science and Engineering, Shibaura Institute of Technology, 3-7-5 Toyosu, Koto-ku, Tokyo 135-8548, Japan

Research Paper

Cite this article: Tanaka S, Oda T, Saiki K (2019). Novel DC-biasing circuits with arbitrary harmonics-control capability for compact high-efficiency power amplifiers. *International Journal of Microwave and Wireless Technologies* **11**, 618–624. https://doi.org/10.1017/S1759078719000473

Received: 14 November 2018
Revised: 18 March 2019
Accepted: 18 March 2019
First published online: 22 April 2019

Key words:
Power amplifiers; Class-F amplifiers; Power-added efficiency; Harmonic tuning techniques; Composite right-/left-handed transmission lines; DC-biasing circuit; Dispersion diagram

Author for correspondence:
S. Tanaka, E-mail: s-tanaka@shibaura-it.ac.jp

Abstract

The next generation mobile communication systems impose challenging performance, size, and cost requirements on the power amplifiers (PAs). This paper presents novel DC-biasing circuits, which are compact and yet can control the harmonics almost arbitrarily. The proposed circuit consists of a composite right-/left-handed (CRLH) transmission line (TL) stub, of which the size and harmonics-control function can be tuned by modifying the dispersion diagram of the stub line. As a proof of concept, a compact 2-GHz 7-W GaN HEMT class-F PA using the versatile CRLH-TL stubs was fabricated, demonstrating 85.8% drain efficiency and 77.3% power-added efficiency.

Introduction

With the advancement of a mobile wireless system, the modulation scheme is becoming increasingly complex. In order to amplify the modulated signal without distorting the high PAPR (Peak-to-Average Power Ratio) waveform, the power amplifiers (PAs) are required to operate in the linear input power range. For classical amplifiers (with fixed load line and constant DC bias voltage), this implies that the overall efficiency is sacrificed because the PAs must be used under backed off conditions to assure linear operation for any instantaneous input power drive. In this respect, Doherty amplifiers and envelope tracking (ET) amplifiers, capable of modulating the load line and the dc bias voltage according to the input power level, respectively, are attracting wide attention as one of the most practical efficiency-enhancement technique to date. For further efficiency improvement, using harmonically tuned power cells have been shown to boost up the efficiency of both the Doherty [1] and ET amplifiers [2]. However, the harmonic tuning circuits, such as those used in class-F amplifiers, could increase the size and cost of the PAs which are already complicated with the sophisticated modern architectures, unless effective measures are taken to miniaturize and simplify the circuitry. Recently, we have demonstrated extremely compact harmonic tuning stubs using composite right-/left-handed (CRLH) transmission lines (TLs) [3]. Despite the small size of the harmonic tuning stub, however, the DC-biasing circuits using quarter-wavelength microstrip line (MSL) stubs still took up a large area, hindering further miniaturization of the whole amplifier circuit. The conventional DC-biasing circuits also have the drawback of spurious 2nd harmonic response, thus restricting the freedom of designing harmonically tuned amplifiers.

In this paper, we present a novel DC-biasing circuit realized using a compact CRLH TL stub. We show that by engineering the dispersion diagram of the CRLH TL, the DC-biasing circuit can generate arbitrary set of transmission zeros (TZs) that can be used to realize class-F load conditions, i.e. short and open for the 2nd and 3rd harmonics, respectively. The stub can also be designed to generate reflection zeros (RZs) at the harmonic frequencies such that the stub behaves like an ideal DC-biasing circuit without spurious harmonic responses. This can simplify the difficult task of optimizing the impedance matching network with harmonic treatment while minimizing the circuit size. To verify the practicability of the proposed technique, a 2-GHz class-F GaN HEMT PA exploiting the proposed DC-biasing circuits is demonstrated.

Design and characterization of DC-biasing circuit

Basic configuration

Figure 1 illustrates the $|S_{21}|$ characteristics for different configurations of the CRLH TL stub. Also shown in the figure are the dispersion diagrams for the CRLH stub lines. The uniqueness of the CRLH TL stub that we have been using lies in the use of the negative-order resonances (NORs) that occur in the left-handed (LH) region of the CRLH TL. Since the property of the electromagnetic wave in the LH region is predominantly determined by the inductors and

© Cambridge University Press and the European Microwave Association 2019

CAMBRIDGE UNIVERSITY PRESS

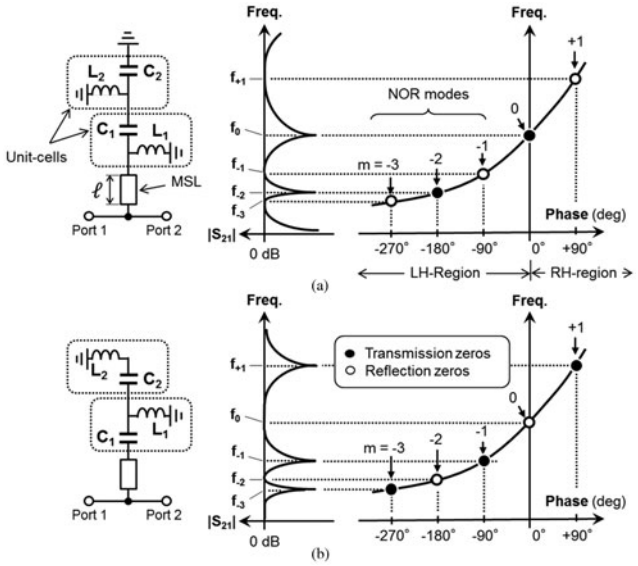


Fig. 1. Schematic illustration of the $|S_{21}|$ characteristics and dispersion diagram for CRLH TL stubs with (a) L-first and (b) C-first configurations.

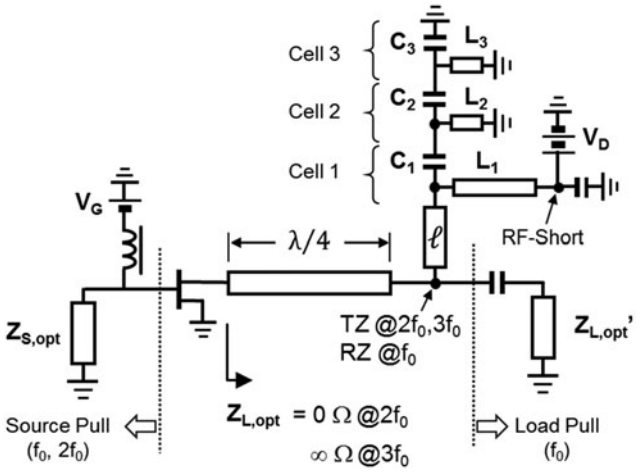


Fig. 2. Basic configuration of the class-F amplifier using the proposed DC-biasing circuit.

capacitors constituting the unit cells, the TZs and the RZs due to the NORs can be arbitrarily controlled by tuning the LC elements.

The frequencies of the NOR are obtained, in general, by numerical calculation. However, if the length of the MSL section of the stub is zero ($\ell = 0$), analytical formulas can be obtained [4]. For example, in the case of the C-first CRLH TL stub with two unit cells (Fig. 1(b)), the resonant frequency of $m = -2$ mode can be obtained as

$$f_{-2} = 1/2\pi\sqrt{(L_1 + L_2)C_2}. \quad (1)$$

The analytical expressions for the $m = -1$ and $m = -3$ modes are also available but with somewhat more complicated formulations [4]. The formulas for the L-first CRLH TL stub with two unit cells (Fig. 1(a)) can also be derived, such as:

$$f_{-2} = 1/2\pi\sqrt{(C_1 + C_2)L_2}. \quad (2)$$

Although the analytical formulas for the special case ($\ell = 0$) do not apply to general cases of $\ell > 0$, they provide a means for roughly estimating the L and C values necessary for obtaining the TZs and RZs at the targeted frequencies.

In designing a CRLH TL stub, there are two design options: looking from the connection point of the stub, the first is to place the shunt inductor first (Fig.1(a)), and the second is to place the reactive elements the other way around (Fig.1(b)). The fundamental resonance modes of the lowest frequency provide a RZ and a TZ for the CRLH TL stubs of "L-first" and "C-first" types, respectively. Since the same applies to the short-ended and open-ended MSL stubs, it can be understood that the CRLH TL stubs of the L-first type and C-first type correspond to conventional short-ended and open-ended MSL stub, respectively.

Now, from Fig. 1(a), it can be seen that the L-first type CRLH TL stub can potentially be used as a DC-biasing circuit by feeding the DC bias via the shunt inductor nearest to the main signal line. Figure 2 shows a typical use case of the proposed CRLH TL stub as a drain DC-biasing circuit for a class-F amplifier. As shown in Fig. 1(a), the RZ of the lowest frequency produced by the L-first CRLH TL stub serves as the passband for the fundamental frequency of the amplifier, as in the case of conventional DC-biasing circuit. Since the inductor line for L_1 is not just a DC feed path but a critical element determining the RF characteristics of the stub, a shunt capacitor is used to define the length of the inductor line RF-wise.

Circuit design method

Dispersion diagram

The characteristics of TL stubs are determined by the phase of the stub lines. Thus, the dispersion diagram (the relationship between the phase and frequency of the TL) provides an effective tool for analyzing the behavior of the TL stubs. However, dispersion diagrams for TLs are normally defined for TLs as two-port circuits. Let us consider the case for a lossless MSL with characteristic impedance (Z_0) of 50 Ω. In this case, the MSL is perfectly matched to 50-Ω load and the dispersion diagram can be conveniently obtained by calculating the phase of the two-port S-parameter [4]

$$S_{21} = e^{-j\theta_{2P}(f)}. \quad (3)$$

The dispersion diagram obtained this way, however, generally fails to predict the characteristics of a stub using the same MSL if, for example, Z_0 is non-identical with 50 Ω. Thus, a different definition of dispersion diagram is required for TLs as stub lines.

To cope with this problem, in [4] we introduced a dispersion diagram defined for a one-port TL:

$$S_{33} = e^{-j2\theta_{1P}(f)}, \quad (4)$$

where port 3 is defined as the connection point of the stub. Figure 3 shows the calculated dispersion diagram based on (4), i.e. $\theta_{1P}(f)$, for a short-ended lossless MSL stub measuring quarter-wavelength at 1 GHz. Also shown is the calculated $|S_{21}|$ characteristics of the stub using the same MSL. (It is reminded that the $|S_{21}|$ here has no relevance to (3).) It can be seen that $\theta_{1P}(f)$ is a linear function of the frequency if $Z_0 = 50$ Ω. In this case, $\theta_{1P}(f)$ is identical with $\theta_{2P}(f)$ which is commonly used

https://doi.org/10.1017/S1759078719000473 Published online by Cambridge University Press

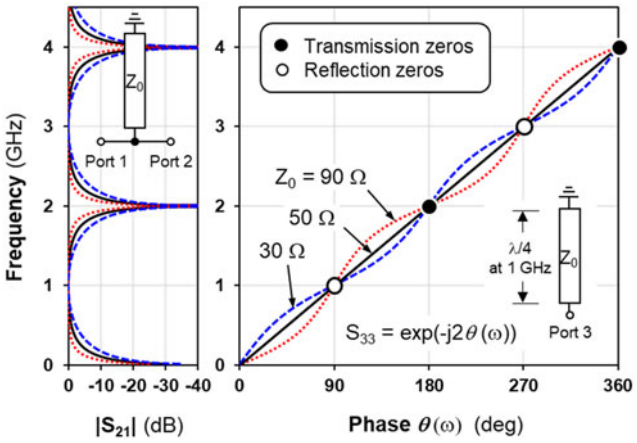


Fig. 3. $|S_{21}|$ characteristics of short-ended MSL stub and corresponding dispersion diagrams for one-port stub lines.

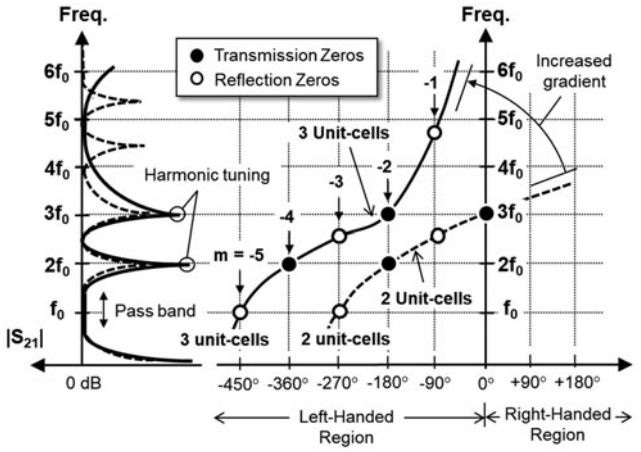


Fig. 4. Schematic illustration of $|S_{21}|$ characteristics and dispersion diagrams for the CRLH TL stubs using two and three unit cells.

for a two-port MSL with the same Z_0 and length. If Z_0 is non-identical with 50 Ω, however, the curvature of $\theta_{1P}(f)$ becomes non-linear. For example, in the case of high impedance stub line ($Z_0 > 50$ Ω), the slope of $\theta_{1P}(f)$ is increased at around the frequencies for RZs at 1 and 3 GHz, increasing the bandwidth of the $|S_{21}|$ characteristics of the stub there. The commonly used DC-biasing circuits based on short-ended quarter-wave stubs thus normally use high characteristic impedance line to increase the bandwidth of the passband for the fundamental RF signal. Similarly, the bandwidth of the $|S_{21}|(f)$ of the stub around the TZs can be increased by using low impedance MSLs ($Z_0 < 50$ Ω). Hereafter, we use the dispersion diagram based on (4) as a tool for designing the CRLH TL stubs.

Design criteria

In general, a CRLH TL to be used as a two-port TL must be designed such that the impedance matching conditions are met for bilateral transmission of the RF signal. To meet the requirements, the CRLH TL is normally configured to have a uniform structure (using identical unit cells) with the balanced and symmetric design. Furthermore, impedance matching is taken into account by adequately choosing the Bloch impedance of the CRLH TL [5]. When designing such CRLH TLs, some key equations for balanced design conditions or Bloch impedance serves as the design criteria and help setting the values for the reactive components of the CRLH TL.

On the other hand, when dealing with a one-port CRLH TL as a stub line, it is not the characteristic impedance (or Bloch impedance) or the uniformity of the TL but the phase that matters. This can be analogically understood by the fact that MSL stubs with non-50-Ω characteristic impedance or stepped impedance [6] are commonly used. Thus, the values for the reactive components of CRLH TL can be varied almost arbitrarily to obtain the desired frequency response of the stub. The CRLH TL can even be non-uniform (using non-identical unit cells), because in the first place periodicity is not a necessity in the CRLH TL theory as long as the homogeneity conditions of the unit cells are met (p.100 in [5]).

Hence, it follows that there are no specific equations serving as design criteria for CRLH TL stubs. As we will see soon, the circuit designer can control the frequency response and even the physical size of the stub by tuning the curvature of the dispersion diagram.

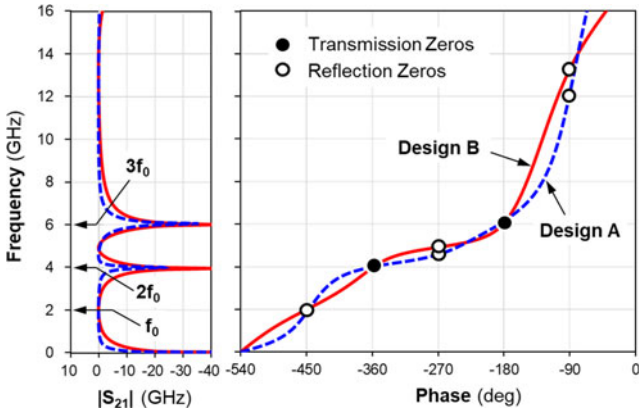


Fig. 5. Calculated dispersion diagrams and $|S_{21}|$ characteristics for CRLH TL stubs with different designs.

Note, however, it is not necessary to do the cumbersome task of computing the dispersion diagram every time the circuit parameters are updated during the optimization process. Instead, practically it just suffices to monitor the $|S_{21}|$ frequency response of the stub while tuning the parameters, because the approximate form of the dispersion diagram $\theta_{1P}(f)$ can be imagined by plotting the phase versus the frequencies of the TZs and RZs which occur alternately with 90° phase interval (see Fig. 1). Although the design method is based on a trial-and-error approach, it is not a burdensome work, unless the initial parameter values are too apart from the solution. In this sense, equations such as (1) and (2) may help setting the initial values.

Circuit size control

The physical dimension of the proposed DC-biasing circuit, consisting of lumped elements and a MSL, is dominated by the length of the MSL section. Thus, to shrink the total size of the DC-biasing circuits, reducing the MSL length is more effective than using less number of unit cells.

Figure 4 shows schematic illustrations of the dispersion diagrams for the CRLH TL stub with two and three unit-cells. The frequencies are in the unit of the fundamental frequency (f_0) of the amplifier. If the number of unit-cells is saved to two, we

https://doi.org/10.1017/S1759078719000473 Published online by Cambridge University Press

Table 1. Design parameter list for CRLH transmission line stubs

Design	C_1 (pF)	C_2 (pF)	C_3 (pF)	L_1 (nH)	L_2 (nH)	L_3 (nH)	ℓ (deg)
A	0.4	0.2	0.1	14.0	1.8	3.2	6.0
B	1.2	0.9	0.6	4.5	0.5	0.5	5.0

need to use the zeroth order resonance (ZOR) mode ($m = 0$) for treating the 3rd harmonic, because only a single TZ (corresponding to NOR mode of $m = -2$) is available in the LH region. This design approach, however, inevitably reduces the gradient of the dispersion curve in the right-handed (RH) region. Since the gradient of the dispersion in the RH region is inversely proportional to the length of the MSL section of the CRLH TL stub, this results in increased size of the whole stub line [7]. For example, in our preliminary design, the MSL section for the case of two unit-cell design measured as long as 16.2 mm which is comparable to the quarter-wavelength of 22.4 mm at 2-GHz.

Now, if we chose to use three unit-cells, five NOR modes including two modes providing TZs ($m = -2, -4$) are available in the LH region. As a result, it becomes possible to let the two NOR modes take care of the 2nd and 3rd harmonics while exploiting the ZOR mode for controlling the dispersion gradient in the RH region. As can be seen from Fig. 4, the ZOR mode (yielding TZ) is tuned to very high-frequency range while fixing the frequency for the two NOR modes ($m = -2, -4$) at the 2nd and 3rd harmonics. This is equivalent to increasing the dispersion gradient and thus to shrink the MSL section of the stub. By using three unit-cell design, the length of the MSL section was reduced from 16.2 mm to 2.5 mm. This is clearly showing the advantage of the CRLH TL stubs designed using the NOR modes, namely, the frequency characteristics and the size can be controlled independently by maneuvering the dispersion diagram in the LH and RH region, respectively.

Bandwidth control

In order for the PA to operate with high power efficiency over a certain frequency range, the frequency variation of the load impedance must be minimized not only at the fundamental frequency band but also at the harmonic frequency bands. As discussed in the previous section, the local gradient of the dispersion diagram directly affects the local bandwidth of the stub frequency characteristics. Thus, the curvature of the dispersion diagram needs to be adequately modified to meet the bandwidth requirements.

Figure 5 compares two dispersion diagrams for CRLH TL stubs with different designs (A and B) for f_0 of 2 GHz. The diagrams were calculated using Keysight ADS circuit simulator based on ideal lumped elements and TLs. Table 1 lists the parameter values used for the two types of design. It can be seen that the dispersion diagram for Design A is optimized for increased bandwidth at around f_0, whereas in Design B more emphasis is placed on increasing the bandwidth at around $2f_0$ and $3f_0$. Also shown in Fig. 5 is the $|S_{21}|$ characteristics for the CRLH TL stubs. It can be seen that comparing the two designs, the bandwidths around the harmonic frequencies are increased for the stub based on Design B.

Experimental results

To confirm the validity of the proposed DC-biasing circuit, two stand-alone CRLH TL stubs with different designs were fabricated and tested. The layout of the CRLH TL stub, initially designed using ADS circuit simulator, was optimized using Momentum EM simulator.

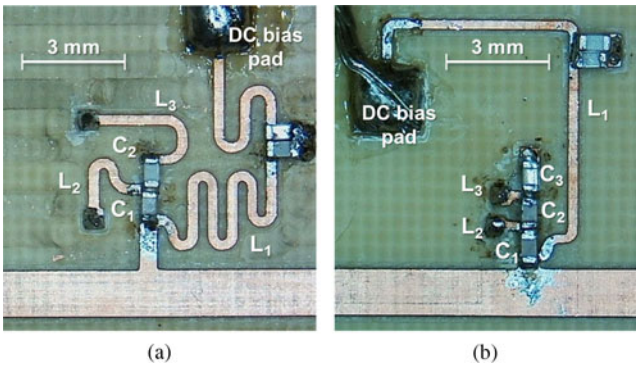


Fig. 6. Photograph of the fabricated DC-biasing circuits of (a) Design A and (b) Design B.

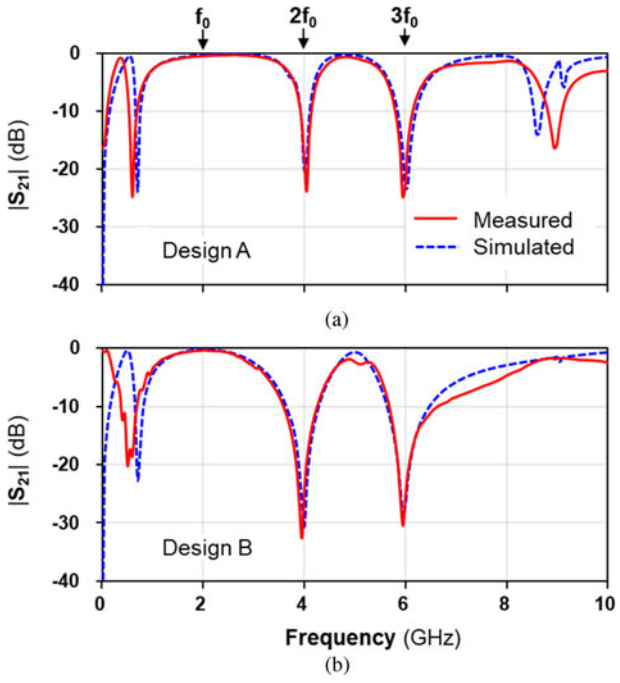


Fig. 7. $|S_{21}|$ characteristics of the DC-biasing circuits.

Figure 6 shows the pictures of the DC-biasing circuits fabricated on Panasonic R-5775 substrate ($h = 0.63$ mm, $\varepsilon_r = 3.6$, tan $\delta = 0.002$). The circuit serving both as a DC-biasing circuit and harmonic tuning circuit can be seen to be very compact, considering that the lengths for the conventional MSL stubs for DC biasing and $2f_0/3f_0$ harmonics tuning are $\lambda/4$, $\lambda/8$, and $\lambda/12$, respectively ($\lambda/4$ equals 22.4 mm at 2 GHz under the same

https://doi.org/10.1017/S1759078719000473 Published online by Cambridge University Press

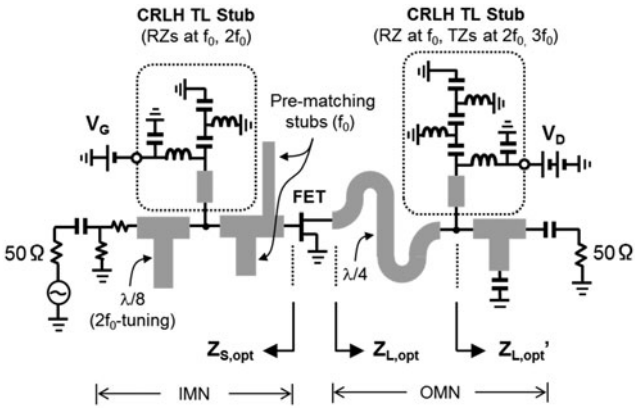


Fig. 8. Configuration of class-F PA using the proposed DC-biasing circuits.

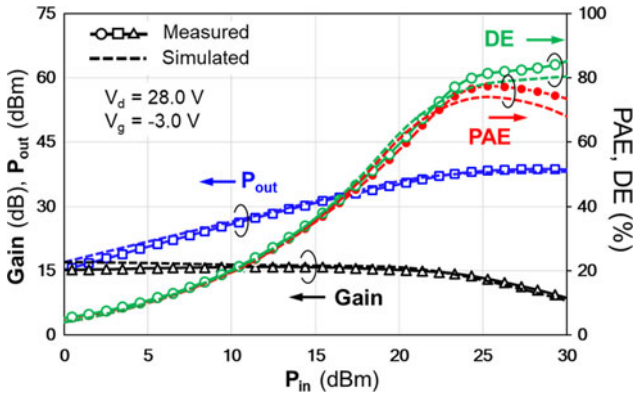


Fig. 11. Power performance of the fabricated 2-GHz PA.

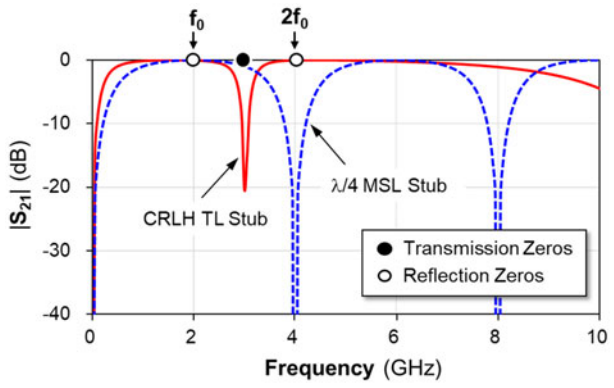


Fig. 9. Simulated $|S_{21}|$ characteristics of the gate DC-biasing circuit.

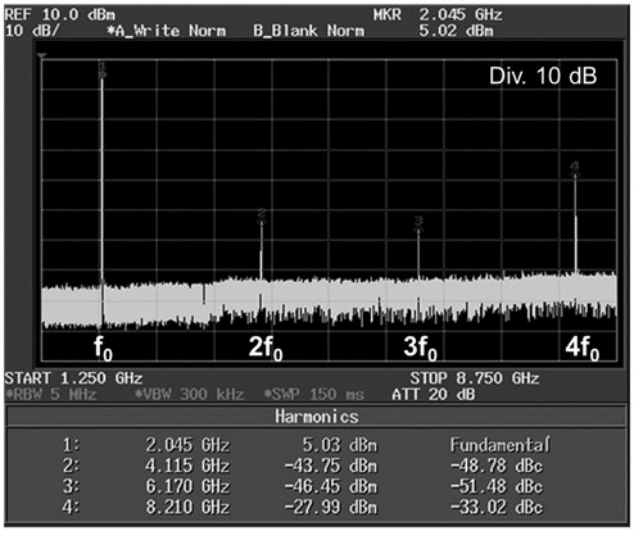


Fig. 12. Output spectrum of the fabricated 2-GHz PA.

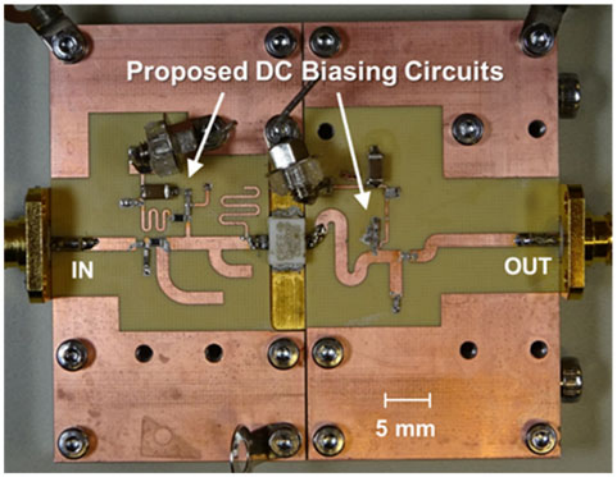


Fig. 10. Photograph of the fabricated 2-GHz PA.

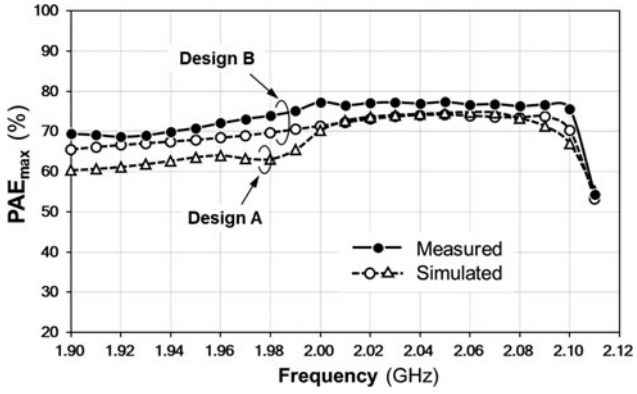


Fig. 13. Frequency dependence of the maximum PAE for PAs with different designs.

conditions). As for the lumped elements for the CRLH TL stub, 1005-size multilayer ceramic capacitors and short-ended MSLs were used for capacitors and inductors, respectively. Care was taken to keep the capacitance values to <1.5 pF so that the self-resonance frequency of the capacitors is sufficiently higher than the 3rd harmonic frequency. Even so, for accurate design, the non-ideal behaviors of the chip capacitors were taken into account in the simulation by using the capacitor models provided by the manufacturer. It can be seen that no capacitor is actually used for C_3 in the circuit of Design A. This is because this design required only a minimum capacitance value of around 0.1 pF

https://doi.org/10.1017/S1759078719000473 Published online by Cambridge University Press

Table 2. Comparison of S-band GaN FET PAs with output power of <12W

Frequency (GHz)	PA design	P_{out} (W)	DE (%)	PAE (%)	V_d (V)	Harmonics tuned	Ref.
2.0	Class-R	10.0	81	76	40	$2f_0$, $3f_0$	[9]
2.22	Class-E	8.9	91	80	28	$2f_0$, $3f_0$	[10]
2.0	Class-J	11.2	–	77.1	28	$2f_0$, $3f_0$	[11]
3.1	Class-F	10.0	85	82	28	$2f_0$, $3f_0$, $4f_0$	[12]
2.0	↑	7.2	85.8	77.3	28	$2f_0$, $3f_0$	This work

for C_3 (Table 1), so a fringing capacitor at the end of the MSL could reasonably be used as a substitute of C_3.

Figure 7 shows the measured $|S_{21}|$ characteristics of the fabricated circuits. During the measurements, the circuits were connected to the DC source via the DC bias pads. It can be seen that both types of CRLH TL stubs generate a RZ at f_0 and TZs at $2f_0$ and $3f_0$. Good agreement between the measurement and EM simulation was obtained at least up to around 8 GHz. Comparing the characteristics of the two designs, it can be seen that there is a tradeoff between the bandwidth at f_0 and the bandwidth at $2f_0$ and $3f_0$. In the next section, we will discuss how the different designs affect the amplifier performance.

Application to class-f PA

Amplifier design

A 2-GHz class-F PA using the proposed DC-biasing circuits was designed. For simulation, a non-linear model for GaN HEMT device (CGH40006P) from Cree Inc. was used. Figure 8 shows the configuration of the class-F PA. Once the design of the proposed DC-biasing circuit was finalized, the load impedances for $2f_0$ and $3f_0$ are determined by the harmonic tuning section of the output matching network (OMN). So, unlike the usual load-pull analysis, we obtained the optimum f_0 load impedance for the FET including the harmonic tuning section of the OMN, as shown in Fig. 2. This method turned out to improve the convergence time of the load-pull simulation as well as the uniqueness of the solution.

The optimum source impedance ($Z_{S,opt}$) for 2 and 4 GHz thus obtained were $1.0 + j2.9\ \Omega$ and $-j23.1\ \Omega$, respectively, at the bias conditions of $V_{gs} = -3.0$ V and $V_{ds} = 28$ V. Meanwhile, the optimum load impedance $Z_{L,opt}$ was $18.6 - j17.2\ \Omega$ at 2 GHz, which led to a simple f_0 impedance matching circuit consisting of a single stub. Conventional harmonic tuning circuits using MSL stubs for class-F amplifiers affect the f_0 load impedance [7], which occasionally results in difficult conditions for matching the impedance at f_0. In this respect, the CRLH TL harmonic tuning stub designed to yield RZ at f_0 has no influence on the f_0 impedance, which is another merit of using CRLH TL stub as a harmonic tuning stub.

As for the input matching network (IMN), various configurations were compared in terms of the circuit size. If the harmonic were to be terminated in short prior to f_0 impedance matching, as usual, the footprint of the IMN became large because significantly long TL was required by the above-mentioned optimum $2f_0$ source impedance. We finally found that the most space-efficient solution is an IMN shown in Fig. 8. Namely, starting from the gate terminal of the FET, we firstly placed the pre-matching stubs for f_0, followed by CRLH TL stub for DC-biasing, $2f_0$ tuning stub and a series capacitor for finalizing the f_0 impedance matching.

Figure 9 shows the simulated $|S_{21}|$ characteristics for the CRLH TL stub designed for gate biasing. The configuration of the CRLH TL stub is shown in Fig. 8. Only two unit cells were used for this particular biasing circuit because only the 2nd harmonic impedance was to be controlled. Based on a similar design method as in the case at the drain side, two RZs and a TZ of NOR modes are placed at f_0, $2f_0$, and at some frequency point in between f_0 and $2f_0$, respectively. As a result, unlike the conventional DC-biasing circuit using $\lambda/4$ stub, the present circuit does not have a harmonic spurious response at $2f_0$. Instead, it provides passbands at f_0 and $2f_0$, and thus can be placed before the $2f_0$ tuning stub without disturbing the harmonic impedance. The present CRLH TL stub for gate biasing is not intended for providing harmonic short (TZ) at $2f_0$. Hence, it was designed based on an approach similar to the case of the drain biasing circuit of Design A (wider bandwidth for the passband).

Measurement results

Figure 10 shows the photograph of the fabricated PA. Compared with the MSL quarter-wavelength of 22.4 mm at 2 GHz, the CRLH TL stub can be seen to be compact in size taking up only small area of the whole circuit. Unconditional stability of the amplifier was assured by using series and shunt resistors in the IMN.

Figure 11 plots the measured power performance of the amplifier at the biasing conditions of $V_{gs} = -3.0$ V and $V_{ds} = 28$ V. The maximum power-added efficiency (PAE) was 77.3% when the drain efficiency (DE) and the output power were 85.8% and 38.6 dBm, respectively.

Figure 12 shows the output spectrum of the amplifier measured at the input drive conditions of 3-dB backed off from saturation. It can be seen that the 2nd and 3rd harmonics are suppressed with regard to the fundamental frequency by −48.8 and −51.5 dB, respectively, whereas the suppression for the 4th harmonic (not treated in the present PA design) is −33.0 dB. The results are an indirect indication of the successful class-F harmonic operation of the amplifier using the proposed DC-biasing circuits.

Discussion

Modern mobile communication system requires high-efficiency operation of the PAs over a wide frequency range. Figure 13 compares the frequency dependence of the maximum PAE for two PAs using drain biasing circuits based on "Design A" and "Design B". As can be seen, the simulation predicts that the PA with "Design B" maintains high PAE (>65%) over wider bandwidth than the PA with "Design A". The measured results for the PA based on Design B shows a similar frequency dependence of maximum PAE. The sharp decrease in PAE at 2.11 GHz results from the 2nd harmonic source impedance approaching the worst impedance conditions point which tends to be located close to the 2nd harmonic optimum source impedance [8].

https://doi.org/10.1017/S1759078719000473 Published online by Cambridge University Press

Table 2 summarizes the power performance of S-band GaN FET PAs with moderate output power (<12 W) [9–12]. The power efficiencies achieved with the present compact PA compares favorably well with those of the state-of-the-art PAs.

Finally, although the present work only addressed the effect of the proposed DC-biasing circuit on the efficiency, the technique could also be useful for improving the linearity with a compact circuit size. For example, studies have shown that the 2nd harmonic tuning at the gate side improves the linearity of the PAs [13]. Thus, the CRLH-TL-based DC-biasing circuits with controlled harmonic responses are expected to increase the circuit design freedom for improving the linearity as well.

Conclusion

Novel DC-biasing circuits based on CRLH TL and their applications to compact harmonically tuned PAs were presented. The proposed circuits take advantage of the strongly nonlinear dispersion diagram of the CRLH TL stub, which becomes possible by using the NORs in the LH region. Two design examples for the versatile DC-biasing circuit were presented. One is the DC-biasing circuit that can also be used as harmonic tuning circuit for class-F amplifier and the other is the one that almost appears to be an ideal DC-biasing circuit without spurious harmonic responses. Taking advantage of the unique properties of the CRLH TL stub based on the NORs, the proposed DC-biasing circuit should be able to be tuned for even wider applications. The class-F PA fabricated in this work showed promising results for applications to more advanced PAs requiring high circuit integration level with minimum circuit size.

Acknowledgements. The authors would like to thank Prof. Kazuhiko Honjo for helpful advice.

References

1. **Colantonio P, Giannini F, Giofre R and Piazzon L** (2009) Theory and experimental results of a Class F AB-C Doherty power amplifier. *IEEE Microwave Theory and Techniques* **57**, 1936–1947.
2. **Mokhti ZA, Tasker PJ and Lees J** (2014) *Using Waveform Engineering to Optimize Class-F Power Amplifier Performance in an Envelope Tracking Architecture*. Rome: European Microwave Integrated Circuits Conference.
3. **Tanaka S, Koizumi S and Saito K** (2016) *Compact Harmonic Tuning Circuits for Class-F Amplifiers using Negative Order Resonance Modes of CRLH Stub Lines*. London: European Microwave Conference.
4. **Tanaka S, Mukaida K and Takata K** (2015) Compact stub resonators with enhanced Q-factor using negative order resonance modes of non-uniform CRLH transmission lines. *IEICE Transactions on Electronics* **E98-C**, 252–259.
5. **Caloz C and Itoh T** (2006) *Electromagnetic Metamaterials: Transmission Line Theory and Microwave Applications*. John Wiley & Sons, Inc., Hoboken, New Jersey.
6. **Chu Q-X and Tian X-K** (2010) Design of UWB bandpass filter using stepped-impedance stub-loaded resonator, IEEE Microw. *Wireless Components Letters* **20**, 501–503.
7. **Tanaka S, Saito K, Oka T and Shibosawa Y** (2017) Applications of dispersion-engineered composite right-/left-handed transmission line stubs for microwave active circuits. *IEICE Transactions on Electronics* **E100-C**, 866–874.
8. **Enomoto J, Ishikawa R and Honjo K** (2017) Second harmonic treatment technique for bandwidth enhancement of GaN HEMT amplifier with harmonic reactive terminations. *IEEE Transactions on Microwave Theory and Techniques* **65**, 4947–4952.
9. **Yao T, Ishikawa R and Honjo K** (2013) *Frequency Characteristic of Power Efficiency for 10 W/30W-Class 2 GHz Band GaN HEMT Amplifiers with Harmonic Reactive Terminations*. Seoul: Asia-Pacific Microwave Conference.
10. **Thian M, Barakat A and Fusco V** (2015) High-efficiency harmonic-peaking class-E power amplifiers with enhanced maximum operating frequency. *IEEE Transactions on Microwave Theory and Techniques* **63**, 659–671.
11. **Wang Y and Larsen T** (2015) *Design of a High-Efficiency GaN HEMT RF Power Amplifier*. Iasi: International Symposium on Signals, Circuits and Systems.
12. **Chen K and Peroulis D** (2013) A 3.1-GHz class-F power amplifier with 82% power-added-efficiency, IEEE Microw. *Wireless Components Letters* **23**, 436–438.
13. **Watanabe S, Takatsuka S, Takagi K, Kuroda H and Oda Y** (1996) Effect of source harmonic tuning on linearity of power GaAs FET under class AB operation. *IEICE Transactions on Electronics* **E79-C**, 611–616.



Shinichi Tanaka received the B.E. and M.E. degrees in applied physics from the University of Tokyo and the D.E degree in Electrical Engineering from Tohoku University in 1984, 1986, and 1997, respectively. In 1986, he joined Central Research Laboratories, NEC Corporation, where he was involved in the development of GaAs and InP HBTs and their applications to microwave and millimeter-wave MMICs. From 1992 to 1993, he was at Purdue University, IN, USA, as a Visiting Scholar. From 2005 to 2009, he was a Visiting Professor at the University of Electro-Communication. Since 2009, he has been a Professor at the Department of Information and Communications Engineering, Shibaura Institute of Technology, Tokyo. His current research interests include microwave power amplifiers, low phase-noise oscillators, and rectifiers for microwave power transmission. Dr. Tanaka is a senior member of the IEEE, IEICE, and IEEJ.



Tomoya Oda received the B.E. degree in Communications Engineering in 2017 and the M.E. degree in Electrical Engineering and Computer Science in 2019, both from Shibaura Institute of Technology. Mr. Oda is a member of the IEICE. Since 2019, he is with Murata Manufacturing Co., Ltd.



Kento Saiki received the B.E. degree in Electrical Engineering in 2017 and the M.E. degrees in Electrical Engineering and Computer Science in 2019, both from Shibaura Institute of Technology. Mr. Saiki is a member of the IEICE. Since 2019, he is with Mitsubishi Electric Corporation.

https://doi.org/10.1017/S1759078719000473 Published online by Cambridge University Press